Large Eddy Simulation of Turbulent Rayleigh-Bénard Convection in a Cubic Cell

N. Foroozani, J. J. Niemela, V. Armenio, and K. R. Sreenivasan

1 Introduction

Turbulent Rayleigh-Bénard convection (RBC) in a fluid heated from below and cooled from above is a challenging problem in nonlinear physics, with many important applications in natural and engineering systems. Because of the complexity of the governing equations, analytical progress in understanding convection has been slow, and laboratory experiments and numerical simulations have assumed increased importance. The RB system is characterized by three non-dimensional parameters: the Rayleigh number Ra $(= \alpha g \Delta T H^3/\nu\kappa)$, the Prandtl number Pr $(= \nu/\kappa)$, and the aspect ratio Γ $(= L/H)$. Here, α is the thermal expansion coefficient, ΔT is the temperature difference between the horizontal plates of height H, g is the acceleration of gravity, κ and ν are the thermal diffusivity and kinematic viscosity of the fluid, respectively, and L is the horizontal extension of the domain.

The subject of turbulent convection has been studied extensively in the past and mostly focused on the main flow features and heat transfer in a cylinder varying the parameters (Ra, Pr, Γ) but only a few of them focused on 3-dimensional complex geometries. Daya & Ecke [1] –henceforth DE01– investigated the influence of the shape of the container on statistics of the convective flow. They found that global parameters such as the Nusselt number, Nu, are not affected by the *geometrical shape*

N. Foroozani · J. J. Niemela
The Abdus Salam International Centre for Theoretical Physics (ICTP), Strada Costiera 11, 34151 Trieste, Italy, e-mail: nforooza@ictp.it, niemela@ictp.it

V. Armenio
Dipartimento di Ingegneria e Architettura, Università di Trieste, 34100 Trieste, Italy, e-mail: armenio@dica.units.it

K. R. Sreenivasan
Departments of Physics and Mechanical Engineering, and the Courant Institute of Mathematical Sciences, New York University, NY 10012, USA e-mail: katepalli.sreenivasan@nyu.edu

of the container but significant differences were observed in the local properties of power law scaling with *Ra*.

The aim of our study is to shed light on previously reported experimental results, DE01, that the scaling of turbulent fluctuations in the geometric center of the convection cell are strongly influenced by the geometrical shape of the convection cell and confirm its validity.

2 Numerical method

We performed large-eddy simulations (LES) to separate the flow field into a resolved (large) scale and a subgrid-scale (SGS) by a spatial filtering operation whose width is proportional to the cell size, $\bar{\Delta} = (\Delta_x \Delta_y \Delta_z)^{1/3}$. The governing equations under the Boussinesq approximation are;

$$\frac{\partial \overline{u}_j}{\partial x_j} = 0, \tag{1}$$

$$\frac{\partial \overline{u}_i}{\partial t} + \frac{\partial \overline{u}_j \overline{u}_i}{\partial x_j} = -\frac{1}{\rho_0}\frac{\partial \overline{P}}{\partial x_i} + \nu \frac{\partial^2 \overline{u}_i}{\partial x_j \partial x_j} - \frac{\overline{\rho}}{\rho_0} g \delta_{i2} - \frac{\partial \tau_{ij}}{\partial x_j}, \tag{2}$$

$$\frac{\partial \overline{\rho}}{\partial t} + \frac{\partial \overline{u}_j \overline{\rho}}{\partial x_j} = k \frac{\partial^2 \overline{\rho}}{\partial x_j \partial x_j} - \frac{\partial \lambda_j}{\partial x_j}, \tag{3}$$

where the symbol $(^-)$ denotes the filtering operation, $\overline{u}_i$ is the velocity component in $i-$direction, x_i is the spatial coordinate in the $i-$direction with x_2 as the vertical (upward) direction, $\overline{P}$ is the pressure field, t is time, and δ_{ij} is the Kronecker symbol. τ_{ij} and λ_j are SGS stress tensor and the SGS heat flux, respectively. In the model it is assumed that density ρ depends linearly on temperature as $\rho = \rho_0[1-\alpha(T-T_0)]$, where ρ_0 is the density at the reference temperature T_0. The effect of the unresolved small scales appears through the terms $\tau_{ij} = \overline{u_i u_j} - \overline{u}_i \overline{u}_j$ and $\lambda_j = \overline{u_j \rho} - \overline{u}_j \overline{\rho}$ in the momentum and density equations, respectively. We use a dynamic eddy viscosity model to parametrize the SGS momentum and buoyancy fluxes as described in Armenio & Sarkar [2]. The model is treated according to the Lagrangian technique proposed by Meneveau *et al.* [3]. It should be noted that our LES methodology has been validated against DNS results of [4] for the case of two infinite and parallel plates, obtaining an excellent agreement for the first-and second-order statistics. We apply the no-slip condition on all six walls. The vertical lateral walls are perfectly adiabatic $\partial \overline{\rho}/\partial \mathbf{n} = 0$, where $\mathbf{n}$ is the normal vector, and the top and bottom walls are isothermal with a fixed temperature difference ΔT giving a density difference $\Delta\rho/\rho_0 = 1$. The aspect ratio of the container is taken to be one. We confine our study to $Pr = 0.7$, which is a typical Prandtl number for air. The equations are discretized on a non-staggered mesh using a second-order-accurate finite difference method. The Adams-Bashforth technique is used for the time advancement of the convective terms, whereas the diffusive terms are treated with the Crank-Nicolson scheme. The Poisson equation is solved using a multi-grid method. A typical domain size is

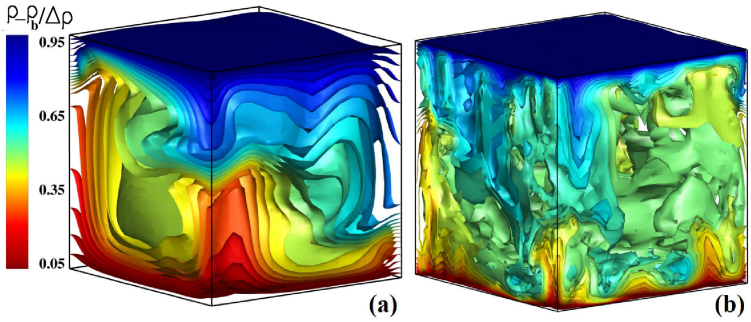

Fig. 1 Instantaneous density iso-surface for (a) $Ra = 10^6$ and (b) $Ra = 10^8$, $Pr = 0.7, \Gamma = 1$ on the $32 \times 64 \times 32$ grids

discretized with $32 \times 64 \times 32$ ($\approx 6.5 \times 10^4$) grid cells in x, y and z directions respectively, for $10^6 \leq Ra \leq 10^8$ with increased resolution to $64 \times 96 \times 64$ ($\approx 4.5 \times 10^6$) for higher Ra. In all simulations, the grid spacing is clustered in the regions close to the walls in order to resolve properly the momentum and thermal boundary layers. It is worth mentioning that for all Ra we verified that the number of grid points (N_{BL}) in the thermal boundary layer was larger than 3-5, exceeding the criterion of Verzicco & Camussi [5]. In our study velocity is normalized by the free-fall-velocity $U_f = \sqrt{(\alpha g \Delta T H)}$, t is normalized by the free-fall time $t_f = H/U_f$, and ρ is the density normalized by $\Delta\rho$. In all the numerical runs, data sampling started once the flow was fully turbulent and had become statistically steady. Moreover, individual runs were performed for over $5000t_f$, which is an order of magnitude larger than that typically used in direct numerical simulation (DNS) (see, e.g., [6]). In order to verify the global properties obtained from our simulations, we compare the Nusselt number, $Nu = \frac{H}{\Delta\rho} \frac{\langle \partial\rho(x,z)\rangle_t}{\partial y} |_{wall}$, with numerical and experimental results from the literature. Here $\langle ... \rangle_t$ denotes a time average of the quantity within the brackets. In terms of its scaling with Ra we obtained $Nu = 0.15Ra^{0.29}$ which is in good agreement with experimental result of Qiu & Xia [7] who obtained $Nu = 0.19Ra^{0.28\pm0.1}$ in their cubic container and using water as a working fluid.

3 Results and discussions

3.1 Flow topology

As an example, the instantaneous density iso-surface obtained for two different $Ra = 10^6$ and $Ra = 10^8$ is shown in figure 1. Even though the mean flow is similar in both cases (up-flow region on the left and down-flow region on the right) the shape of

the iso-surfaces changes dramatically with *Ra*. Indeed, the size of the structures decreases rapidly with increasing *Ra*.

3.2 Determination of LSC orientation

Figure 2 illustrates the time-averaged vertical velocity streamlines over *a finite time-interval* in which the orientation of the large-scale circulation (LSC) is known to be stable along one diagonal plane.

The flow exhibits a *mean wind* (or LSC) [8, 7] moving along one of the diagonal directions (see figure 2(a)) with two small recirculation regions in the corners: one is at the top-left corner of the figure where the mean wind coming from below impinges the upper surface of the cavity and the other is at the lower-right corner where the descending mean wind impinges the bottom surface. In the opposite diagonal (figure 2(b)) two strong counter-rotating vortex structures are shown converging at the mid-plane. Such counter-rotating flows have also been observed in other simulations (see, e.g., [6]). This complex flow structure has significant effects on the resulting turbulent fields.

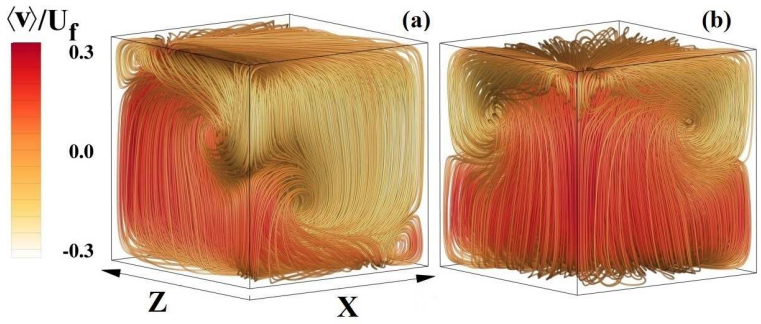

Fig. 2 Streamlines within the full convection cell time averaged for more than $5296t_f$. Colour contour denotes the intensity of the vertical mean velocity, normalized by the free-fall velocity scale $\langle \mathrm{v} \rangle / U_f$. Figure (a) shows one of the diagonals containing the mean wind and (b) shows the opposite diagonal, illustrating strong counter-rotating cells. $Ra = 10^6, Pr = 0.7$ and $\Gamma = 1$ on the $32 \times 64 \times 32$ grids.

3.3 Local fluctuations

We define the root-mean-square (σ) of the resolved density fluctuations as $\sigma_\rho(\mathbf{x}) = [\langle \rho(\mathbf{x})\rho(\mathbf{x}) \rangle_t - \langle \rho(\mathbf{x}) \rangle_t \langle \rho(\mathbf{x}) \rangle_t]^{1/2}$, normalized by $\Delta\rho$, and that of resolved vertical velocity fluctuations as $\sigma_\mathrm{V}(\mathbf{x}) = [\langle \mathrm{v}(\mathbf{x})\mathrm{v}(\mathbf{x}) \rangle_t - \langle \mathrm{v}(\mathbf{x}) \rangle_t \langle \mathrm{v}(\mathbf{x}) \rangle_t]^{1/2}$ normalized by

ν/H. It should be stressed that the SGS contribution to the total *rms* is negligible. The normalized density and velocity fluctuations is shown in figure 3 as a function of *Ra*. The measured fluctuations of density, $\sigma_\rho/\Delta\rho$, are well described at the cell center by the power law $\sigma_\rho/\Delta\rho = 49.03Ra^{-0.46}$ (solid line). The scaling behavior is in excellent agreement with DE01 for a near-cubic cell with $\Gamma = 0.7$ and $Pr = 5.46$.

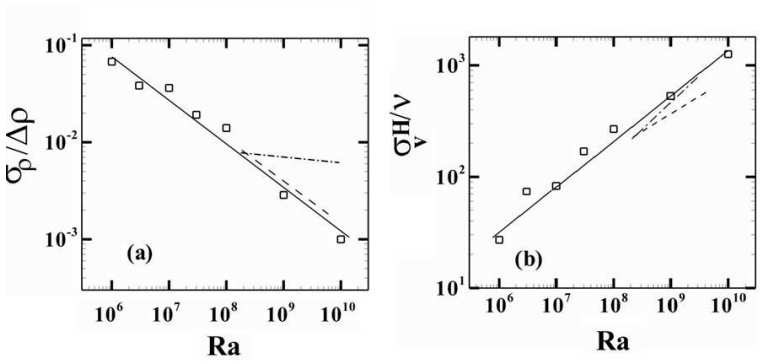

Fig. 3 Normalized fluctuations in (a) density given by $\sigma_\rho/\Delta\rho$ and (b) the vertical velocity given by $\sigma_V H/\nu$ measured at the cell center. The solid line are the power law fits: $\sigma_\rho/\Delta\rho = 49.03Ra^{-0.46}$ (a) and $\sigma_V H/\nu = 0.31Ra^{0.39}$ (b). Dashed lines are power law fits for the near-cubic cell and dash-dotted for the cylindrical cell of DE01 for comparison.

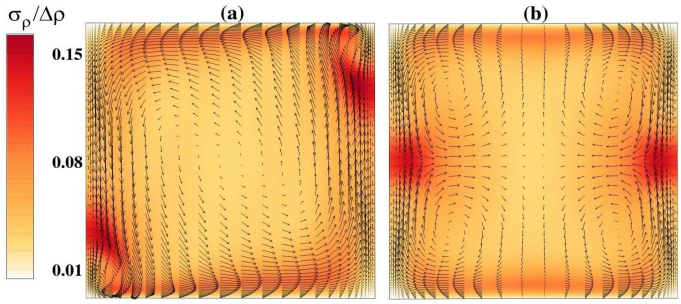

Fig. 4 Time-averaged local *rms* density fluctuation in the units of $\Delta\rho$. $Ra = 10^6$, $Pr = 0.7, \Gamma = 1$. Averaging has been performed over 5296 t_f. Figure (a) shows the vertical diagonal plane containing the large scale circulation and (b) shows the other vertical diagonal plane containing the counter-rotating cells. We have included the velocity vectors for clarity.

Indeed, those authors found a power exponent of -0.48 ± 0.03 (the dashed line in figure 3(a)) while, for cylindrical cells under the same experimental conditions, they measured the considerably smaller exponent of -0.1 ± 0.02 (the dash-dotted line). In figure 3b we show the *rms* velocity fluctuations in our cubic cell and fit it by $\sigma_V H/\nu = 0.31Ra^{0.39}$. This result is also in good agreement with DE01 in which the measured exponent was 0.36 ± 0.05 (dashed line). By way of contrast, their

result for the cylindrical cell, shown again by a dashed-dotted line, demonstrates the large difference resulting from the change in cross-sectional geometry. The data in figure 3 were taken at the cell center. The time-averaged mapping of density fluctuations is shown in figure 4 reveals fixed inhomogeneities in the vertical planes corresponding to the two diagonals. At the mid-height level, the higher levels of *rms* density fluctuations correspond to the diagonal opposite that of the LSC where we observe strong counter-rotating vortex structures (see figure 2) which mix hot and cold plumes at their mid-height convergence (figure 4(b)). Thus it is no surprise that the largest gradient in density fluctuations occurs there.

4 Conclusions

To summarize, we investigated numerically the scaling of the local density fluctuations in RBC in a unit aspect ratio cubic confinement. We observed a stable pattern of LSC for all *Ra* investigated (within a proper time-interval), which has a strong influence on the scaling of fluctuations. Extending the range of *Ra* accessed by DE01, we have confirmed the scaling seen by those authors for both density (temperature) and velocity fluctuations at the cell center and provide insights on physical mechanisms for the observed scaling properties.

References

1. Z. A. Daya and R. E. Ecke, Does turbulent convection feel the shape of geometry? *Phys. Rev. Lett.* **87**, 184501, (2001).
2. V. Armenio and S. Sarkar, An investigation of stably stratified turbulent channel flow using large eddy simulation, *J. Fluid Mech.* **459**, 1, (2002).
3. C. Meneveau, T. S. Lund and W. H. Cabot, A Lagrangian dynamic subgrid-scale model of turbulence, *J. Fluid Mech.* **319**, 353, (1996).
4. S. J. Kimmel and J. A. Domaradzki, Large eddy simulations of Rayleigh-Bénard convection using subgrid scale estimation model, *Phys. Fluids* **12**, 169, (2000).
5. R. Verzicco and R. Camussi, Numerical experiments on strongly turbulent thermal convection in a slender cylindrical cell, *J. Fluid Mech.* **477**, 19, (2003).
6. M. Kaczorowski and K. Q. Xia, Turbulent flow in the bulk of Rayleigh-Bénard convection: small-scale properties in cubic cell, *J. Fluid Mech* **722**, 596, (2013).
7. X. L. Qiu and K. Q. Xia, Viscous boundary layers at the side wall of convection cell, *Phys. Rev. Lett.* **58**, 486, (1998).
8. J. J. Niemela, L. Skrbek, K. R. Sreenivasan and R. J. Donnelly, The wind in confined thermal convection, *J. Fluid Mech.* **449**, 169, (2001).